Thermalization of coupled atom-light states in the presence of optical collisions

I. Yu. Chestnov,[1,*] A. P. Alodjants,[1,†] S. M. Arakelian,[1] J. Nipper,[2] U. Vogl,[2] F. Vewinger,[2] and M. Weitz[2]
[1]*Department of Physics and Applied Mathematics, Vladimir State University, Gorky str. 87, 600000, Vladimir, Russia*
[2]*Institut fur Angewandte Physik der Universität Bonn, Wegelerstraße 8, 53115 Bonn, Germany*
(Received 26 December 2009; published 24 May 2010)

The interaction of a two-level atomic ensemble with a quantized single-mode electromagnetic field in the presence of optical collisions is investigated both theoretically and experimentally. The main focus is on achieving thermal equilibrium for coupled atom-light states (in particular dressed states). We propose a model of atomic dressed-state thermalization that accounts for the evolution of the pseudo-spin Bloch vector components and characterize the essential role of the spontaneous emission rate in the thermalization process. Our model shows that the time of thermalization of the coupled atom-light states depends strictly on the ratio of the detuning to the resonant Rabi frequency. The predicted time of thermalization is in the nanosecond domain at full optical power and about 10 times shorter than the natural lifetime in our experiment. Experimentally we investigate the interaction of the optical field with rubidium atoms in an ultrahigh-pressure buffer gas cell under the conditions of large atom-field detuning comparable to the thermal energy in frequency units. In particular, an observed asymmetry of the saturated lineshape is interpreted as evidence of thermal equilibrium of coupled atom-light states.

DOI: 10.1103/PhysRevA.81.053843 PACS number(s): 42.50.Nn, 05.30.Jp, 32.70.Jz

I. INTRODUCTION

Present remarkable achievements with coherent manipulation of coupled matter-field states evoke great interest in the investigation of phase transitions in such systems; see, for example, [1–3]. The key role in the behavior of coupled states under consideration is played by so-called dark and bright polaritons, that is, bosonic quasiparticles representing a linear superposition of photons in an external (probe) field and the macroscopic (coherent) polarization of a two-level atomic system or excitons localized in quantum wells.

The critical temperature of a phase transition for polaritons can be high enough due to their small effective mass, which is many orders of magnitude smaller than the free mass of atoms (or electrons). Although evidence of Bose-Einstein condensation (BEC) of polaritons in semiconductor microstructures has recently been reported by several groups (see [1], [2], and [4]) observation of the high-temperature phase transition remains an unsolved problem. In this sense atomic systems seem to be more attractive and experimentally feasible for polariton BEC purposes [5–8].

The main difficulty with polariton condensate observation is connected with the problem of achieving true thermal equilibrium for coupled matter-field states, which is a primary step in studying phase transitions in the systems under consideration. Roughly speaking, the polaritonic system for the current experiments with semiconductor microcavities is in nonequilibrium (or quasiequilibrium) (see, e.g., [9]). One mechanism for achieving thermal equilibrium of low-branch polaritons with the host lattice is to cool them with a phonon bath [10]. The thermalization time must be shorter than the polariton lifetime in this case. For the current experiments the lifetime of polaritons is in the picosecond regime and comparable to the thermalization time.

In the area of atomic physics, extremely long lifetimes of excitations are readily achieved at present. In this paper we show that the atomic polariton lifetime is limited by the lifetime of the two-level atomic transition τ_{spont} only, that is, by spontaneous emission. Since the value of τ_{spont} is in the nanosecond regime, the thermalization time can be longer compared with that of polaritons formed in semiconductor devices. Therefore polaritons in an atomic physics system could be preferable for observation of BEC, because of the long coherence times achieved.

Progress toward the achievement of thermal equilibrium in coupled atom-field states was made by some of us in [11]. In particular, the ability to thermalize coupled atom-light (dressed) states due to frequent collisions of rubidium atoms with buffer gas atoms in the presence of optical irradiation has been demonstrated experimentally. In the literature this process is called optical collision (OC) (see, e.g., [12]). We note that redistribution in OCs has also recently allowed laser cooling of ultradense atomic gases [13].

In general atomic collisions in the presence of a laser field can be considered as a scattering (inelastic) process when both the internal (or kinetic) energy of the particles and the energy of the scattered light are changed. Physically this leads to dephasing of the atomic polarization that determines the broadening of the fluorescence spectrum and introduces an additional (collisional) phase shift. Notably, a closed representation to understand the effect of atomic collisions on the resulting width and shape of spectral lines was performed by Weisskopf in his famous paper [14]. Thereafter collisional broadening has been a subject of intensive investigation both in theory and in experiment (see, e.g., [15–18]). Various aspects and approaches to line shape description, phase shift, and intensity due to nonresonant atomic collisions have been studied and summarized in [19]. Notably, important properties of spectral line shift, width, and asymmetry for a wide range

*igor_chestnov@mail.ru
†alodjants@vlsu.ru

of foreign (buffer) atomic gas densities in connection with the so-called impact limit of atomic collisions have been discussed by A. Royer in [18] (see also [17]).

A statistical approach to the OC problem was proposed in [20], based on the cross section of collisionally aided radiative excitation (or emission) for two-level atoms coupled to a thermostat of buffer gas. Subsequently, in [21] the authors established a simple theory of OC based on the dressed-state approach in the Schrödinger picture. It has been shown that collisions with buffer gas particles reduce to a transfer between different dressed states of the atom. Spectral redistribution of quasiresonant radiation occurring due to collisional relaxation has been a subject of experimental investigations as well (see, e.g., [22–24]). The OC spectral line shape is essentially non-Lorentzian, that is, asymmetric. From a molecular point of view, such an asymmetry can be understood by taking into account modifications of interaction potential curves [22,25].

Although the main features of OCs have been investigated for a long time, the thermodynamic properties of coupled atom-light systems have not yet been studied fully. It is pointed out in [12] that, in the limit of a low Rabi splitting energy $\hbar\Omega_R$, that is, for $\hbar\Omega_R \ll k_B T$ (T is the temperature of the two-level atomic ensemble), the OCs reduce to equalizing dressed-state populations under the secular approximation. The deviations from the Einstein coefficients for absorption and stimulated emission induced by OCs are discussed in [26]. However, the problem of thermalization of coupled atom-field states has not been studied. Standard theoretical approaches in this case are based on the rate equations for the population of dressed states only, completely ignoring coupling between population and atomic coherences at the same time (see, e.g., [11], [12], and [26]). Such an approach seems unsuitable if we keep in mind the problem of observation of polariton BEC. Actually spontaneous polarization buildup occurs in this case and polariton coherences become important (cf. [9]). Thus, the role of the secular approximation in the thermalization process of coupled atom-light states should be clarified.

The aim of this report is a fundamental theoretical and experimental investigation of the thermalization of coupled atom-field states, taking into account spontaneous emission processes beyond the approximations typically used.

In Sec. II we establish the model of interaction of two-level atoms with a quantized optical field in the presence of OCs. Realistic (experimentally accessible) conditions for OC of rubidium atoms with high-pressure buffer (argon or helium) gas atoms are discussed. In Sec. III the Bloch-like equations for density matrix elements in the dressed-state basis are derived. Analysis of the steady-state solutions of these equations is performed in Sec. IV. We define the time of thermalization and specify necessary conditions to achieve thermal equilibrium for dressed atom-light states. In Sec. V we derive the properties of intensities of spectral components for an atomic system in the presence of OC under the atom-field thermalization process. Thermalization of coupled atom-light states in an ultrahigh-pressure buffer gas environment is experimentally investigated in Sec. VI. The spectrum of fluorescence obtained from rubidium atoms is analyzed. We give an explanation for the observed resonance fluorescence signal and necessary estimations of the time of thermalization according to the theoretical approach developed here. In Sec. VII we summarize our results and discuss further prospects for the experiment and the corresponding theory. In particular, the possibility of polariton condensation is discussed.

II. MASTER EQUATION APPROACH TO ATOM-FIELD INTERACTION IN THE PRESENCE OF OPTICAL COLLISIONS

Atomic collision in the presence of a nonresonant radiation field can be considered as the elementary process of a collision between an isolated two-level atom A and a foreign (buffer) gas atom of sort B; that is,

$$A(a) + B + \hbar\omega_L \leftrightarrows A(b) + B, \tag{1}$$

which occurs with simultaneous emission (or absorption) of a photon with frequency ω_L. The collision is called an OC when the frequency of the optical field ω_L is near resonant to an atomic transition in A. In Fig. 1 schemes of nonresonant absorption of light with frequency ω_L during collision with a buffer gas atom are shown. The case of collisionally aided excitation of level $|b\rangle$ of the atom for negative atom-light detuning, $\delta = \omega_L - \omega_0$, is illustrated in Fig. 1(a). For positive detuning $\delta > 0$ ($\omega_L > \omega_0$), the atom has some energy excess $\hbar\delta$, which is transferred to the kinetic energy of the atoms after the collision [Fig. 1(b)]. Note that for both cases excitation of the upper level $|b\rangle$ is impossible due to atomic collision only.

Our description of thermalization of atom-field (dressed) states developed here is based on the approach to OC presented in [12] and generalizes their treatment to detuning of δ values comparable to or higher than the thermal energy $k_B T$. The master equation for the density matrix σ in the presence of both OCs and radiative (spontaneous) relaxation processes can be written as follows:

$$\frac{d\sigma}{dt} = -\frac{i}{\hbar}[H,\sigma] + \left\{\frac{d\sigma}{dt}\right\}_{\text{rad}} + \left\{\frac{d\sigma}{dt}\right\}_{\text{coll}}, \tag{2}$$

where the last two terms account for spontaneous emission and collisions with buffer gas atoms. The Hamiltonian H describes atom-field interaction under the rotating wave approximation and has the form

$$H = \hbar\omega_L f^\dagger f + \hbar\omega_0 |b\rangle\langle b| + \hbar g(S_+ f + S_- f^\dagger), \tag{3}$$

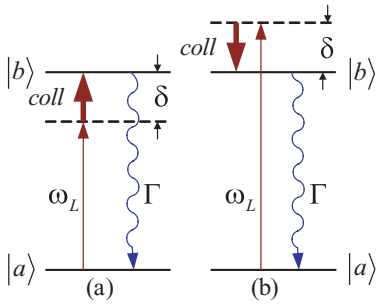

FIG. 1. (Color online) Schematic representation of collisionally aided absorption in a two-level atom with frequency ω_L for (a) negative atom-field detuning, $\delta < 0$, and (b) positive atom-field detuning, that is, $\delta > 0$. The decay Γ is the spontaneous emission rate.

where $f(f^\dagger)$ is the annihilation (creation) operator for the photons absorbed (or emitted) due to atomic collisions, $g = \sqrt{|d_{ab}|^2\omega_L/2\hbar\epsilon_0 V}$ is the atom-field interaction constant, which we take to be identical for all atoms, d_{ab} is the atomic dipole matrix element, and V is the interaction volume. In expression (3) $S_- = |a\rangle\langle b|$ and $S_+ = S_-^\dagger \equiv |b\rangle\langle a|$ represent atomic transition operators. The term

$$\left\{\frac{d\sigma}{dt}\right\}_{\text{rad}} = -\frac{\Gamma}{2}(S_+S_-\sigma + \sigma S_+S_-) + \Gamma S_-\sigma S_+ \tag{4}$$

characterizes the contribution of spontaneous processes in Eq. (2); $\Gamma \equiv 1/\tau_{\text{spont}}$ is the spontaneous emission rate (τ_{spont} is the natural lifetime of the atomic transition). The last term in Eq. (2) describes the atomic collisions and can be established as

$$\left\{\frac{d\sigma}{dt}\right\}_{\text{coll}} = -\frac{\gamma}{2}\sigma + 2\gamma s_z\sigma s_z - i\eta\,[s_z,\sigma]\,, \tag{5}$$

where $s_z = \frac{1}{2}(|b\rangle\langle b| - |a\rangle\langle a|)$ is the atomic population inversion operator obeying conditions $s_z|a\rangle = -\frac{1}{2}|a\rangle$ and $s_z|b\rangle = \frac{1}{2}|b\rangle$.

In (5) parameter γ characterizes the collisional relaxation rate (collisional broadening) in the presence of a monochromatic laser field; η determines the average phase shift appearing due to collisions. In connection with the theory of OC parameters, γ and η can be represented as (cf. [12])

$$\gamma = \langle 1 - \cos\phi\rangle_{\text{coll}}, \tag{6a}$$

$$\eta = \langle \sin\phi\rangle_{\text{coll}}, \tag{6b}$$

where $\phi = \int_{-\infty}^{+\infty}[\omega_{ba}(t) - \omega_0]\,dt$ is the phase shift that accumulates during the collision.

More rigorous expressions for collisional broadening γ can be found using a full quantum mechanical (microscopic) approach (see, e.g., [25]). In general, γ implicitly depends on the atom-field detuning δ and, thus, on the molecular potentials for a compound system. For $\delta = 0$ the magnitude of γ can be inferred from the expression

$$\gamma \simeq \pi\rho_0^2 \mathrm{v_T} N_B, \tag{7}$$

where ρ_0 is the Weisskopf radius, depending on the molecular level variation (shifting) due to atomic collisions, $\mathrm{v_T} = \sqrt{2k_BT/m_{at}}$ is the thermal atomic velocity, and N_B is the number density of the buffer gas.

In particular, in the experiment described in Sec. VI, we use rubidium atoms with mass $m_{\text{at}} \simeq 1.46 \times 10^{-25}$ kg under the temperature $T = 530$ K and a buffer gas of density $N_B \simeq 10^{21}$ cm^{-3}. Taking into account typical values of the Weisskopf radius $\rho_0 \simeq 10^{-3}$ μm for the collisional broadening rate (7), one can obtain a value of a few terahertz. The average collisional shift η can be expressed via molecular level variation under the quantum mechanical description as well. Practically, η in (6b) has the same order of magnitude as a collisional broadening γ. In the current experiment we used argon as the buffer gas ($\gamma/2\pi \equiv \gamma_{\text{Ar}}/2\pi \simeq 7.2$ GHz/bar, $\eta/2\pi \equiv \eta_{\text{Ar}}/2\pi \simeq -6$ GHz/bar) at 500 bar (50 MPa) pressure and helium as the buffer gas ($\gamma_{\text{He}}/2\pi \simeq 2.8$ GHz/bar, $\eta_{\text{He}}/2\pi \simeq 1.6$ GHz/bar) at 400 bar (40 MPa), respectively.

The spontaneous emission rate for experimentally utilized rubidium atom D lines is $\Gamma \simeq 2\pi \times 6$ MHz ($\tau_{\text{spont}} = 27$ ns) (see, e.g., [27]). Thus, condition $\gamma \simeq \eta \gg \Gamma$ is held in the experiment under discussion. Nevertheless, as we will see, spontaneous emission plays an essential role in the thermalization process of coupled atom-light states due to its ability to change the population of the excited atomic level.

Note that the Doppler effect is not important for the problem under consideration. First, the motion of the atoms cannot change the population of atomic levels and, thus, cannot restrict the thermalization process. Second, Doppler broadening (of the order of a gigahertz) is significantly smaller than the collisional broadening in the experiment, thus neglecting the Doppler broadening in our calculations is justified.

Let us now consider the situation when each collision happens in a short enough time span τ_{coll}. In this case two collisions are well separated in time; that is, we have

$$\tau_{\text{coll}} \ll T_{\text{coll}}, \tag{8}$$

where T_{coll} is the time interval separating two collisions. Here we neglect temporal correlations between the spontaneous emission process and the collisional one. Loosely speaking, spontaneous emission and OC processes are well separated in time as well. Further, Eq. (2) is valid under the so-called impact limit of OCs (see, e.g., [12]). The applicability of our model in this case is discussed later.

III. BLOCH-LIKE EQUATIONS UNDER THE DRESSED-STATE REPRESENTATION

In the absence of collisions with buffer gas atoms, Hamiltonian (3) for atom-light interaction explicitly has two eigenstates, called dressed states, defined as

$$|1(N)\rangle = \sin\theta|a,N+1\rangle + \cos\theta|b,N\rangle, \tag{9a}$$

$$|2(N)\rangle = \cos\theta|a,N+1\rangle - \sin\theta|b,N\rangle, \tag{9b}$$

where N is the total photon number, and $|a,N+1\rangle$ and $|b,N\rangle$ are bare atom-light states. The mixing angle $\theta \equiv \theta(\delta)$ is defined by

$$\tan 2\theta = -\frac{\Omega_0}{\delta}, \quad 0 \leqslant 2\theta < \pi, \tag{10}$$

where $\Omega_0 \simeq 2g\sqrt{N}$ denotes the resonant Rabi frequency. In general, the parameters $\sin\theta$ and $\cos\theta$ can be represented as [11]

$$\sin\theta = \frac{1}{\sqrt{2}}\sqrt{1 + \frac{\delta}{\Omega_R}}, \tag{11a}$$

$$\cos\theta = \frac{1}{\sqrt{2}}\sqrt{1 - \frac{\delta}{\Omega_R}}, \tag{11b}$$

where $\Omega_R = \sqrt{\delta^2 + \Omega_0^2}$ is the Rabi splitting frequency. It is important to emphasize that state $|2(N)\rangle$ is always located below state $|1(N)\rangle$.

In Fig. 2 the dependence of dressed-atom-state energies as a function of light frequency ω_L is presented schematically. The frequency gap between dressed states $|1(N)\rangle$ and $|2(N)\rangle$ is the Rabi splitting frequency Ω_R. The gap is minimal and equal to the Rabi frequency $\Omega_{R,\min} = \Omega_0$ under the atom-light resonance condition ($\delta = 0$). In this paper we mostly focus on

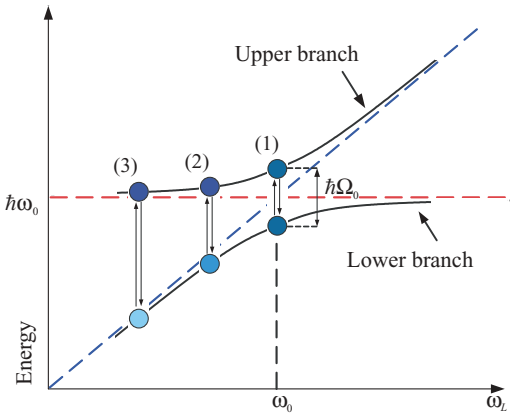

FIG. 2. (Color online) Dispersion relation for coupled atom-light states versus ω_L; $\hbar\Omega_0$ is the resonant Rabi splitting energy. The upper branch corresponds to the $|1(N)\rangle$ dressed state, and the lower branch describes the $|2(N)\rangle$ state. The dashed horizontal line corresponds to the uncoupled level $|b,N\rangle$, that is, to the atomic transition energy $\hbar\omega_0$. The experimentally observed coupled states are states (2) and (3), for which condition (13) is satisfied.

the case for which the Rabi splitting energy is comparable to or higher than the thermal energy; that is,

$$\hbar\Omega_R \geqslant k_B T. \tag{12}$$

For the current experiment (see Sec. VI) we are limited to Rabi frequencies $\Omega_0/2\pi$ by the value of 0.1 THz, which corresponds to full optical power $P_0 \simeq 300$ mW. At the same time the thermal energy ($k_B T$) for rubidium atoms at ambient temperatures ($T = 530$ K) corresponds to a frequency of 11 THz. In this case, we need to have large detuning δ values ($|\delta|/2\pi \geqslant 11$ THz) to fulfill relation (12). In other words, in this paper we are practically interested in the perturbative limit when

$$\Omega_0 \ll |\delta|. \tag{13}$$

Physically condition (13) means that we deal with dressed states situated far from the region of resonant atom-field interaction. In Fig. 2 this situation is labeled (2) and (3) respectively.

We solve the master Eq. (2) in the basis of dressed states $|1(N)\rangle$ and $|2(N)\rangle$. The density matrix elements in the dressed-state representation (9) traced over the photon number N are defined as

$$\sigma_{11} = \sum_N \langle 1(N)|\sigma|1(N)\rangle, \tag{14a}$$

$$\sigma_{22} = \sum_N \langle 2(N)|\sigma|2(N)\rangle, \tag{14b}$$

$$\sigma_{21} = \sigma_{12}^* = \sum_N \langle 2(N)|\sigma|1(N)\rangle. \tag{14c}$$

The matrix elements σ_{11} and σ_{22} describe the populations of the dressed states $|1(N)\rangle$ and $|2(N)\rangle$, respectively. The nondiagonal elements σ_{12} (σ_{21}) characterize dressed-state coherences and correspond to population transfer between dressed-state levels. Notably, the total population of dressed states (14) is conserved for OC processes; that is, we have $d(\sigma_{11} + \sigma_{22})/dt = 0$.

We now consider the properties of the real components $S_{x,y,z}$ of the pseudospin (Bloch) vector $\vec{S}$ combined from matrix elements (14) as follows:

$$S_x = \sigma_{12} + \sigma_{21}, \tag{15a}$$

$$S_y = i\,(\sigma_{12} - \sigma_{21}), \tag{15b}$$

$$S_z = \sigma_{11} - \sigma_{22}. \tag{15c}$$

With the help of (2)–(5) it is possible to get Bloch-like equations for pseudospin components $S_{x,y,z}$,

$$\frac{dS_x}{dt} = -(\Gamma_{\rm coh} + \varsigma)S_x - \tilde{\Omega}_R S_y - 2(\alpha - \Gamma_{12}) \times \left(S_z - \frac{2wS_z^{(\rm eq)}}{(2w + \Gamma_+)}\right) + \Gamma\sin(2\theta), \tag{16a}$$

$$\frac{dS_y}{dt} = -\left(\frac{\Gamma}{2} + \gamma\right)S_y + \tilde{\Omega}_R S_x + 2U\left(S_z - \frac{2wS_z^{(\rm eq)}}{(2w + \Gamma_+)}\right), \tag{16b}$$

$$\frac{dS_z}{dt} = -2w\left[\left(1 + \frac{\Gamma_+}{2w}\right)S_z - S_z^{(\rm eq)}\right] - 2\,(\alpha - \Gamma_{12})\,S_x - 2U S_y + \Gamma_-, \tag{16c}$$

where the following notations are introduced:

$$\alpha = \frac{\gamma\sin(4\theta)}{4}, \quad w = \frac{\gamma\sin^2(2\theta)}{2}, \quad \varsigma = \gamma\cos^2(2\theta), \quad U = \frac{\eta\sin(2\theta)}{2}, \quad \Gamma_{\rm coh} = \frac{\Gamma}{2}[1 + \sin^2(2\theta)], \tag{17a}$$

$$\Gamma_\pm = \Gamma[\sin^4(\theta) \pm \cos^4(\theta)], \quad \Gamma_{12} = \frac{\Gamma\sin(4\theta)}{8}. \tag{17b}$$

In Eqs. (16), $\tilde{\Omega}_R = \Omega_R - \delta\eta/\Omega_R$ is a modified Rabi splitting that takes into account the average phase shift η arising due to collisions with buffer gas atoms. The coefficients $\Gamma_{\rm coh}$, $\Gamma_\pm$, and Γ_{12} in (17b) characterize spontaneous emission in the dressed-state representation. In general they are connected with spontaneous emission rates $\Gamma_{1\to1} = \Gamma_{2\to2} = \frac{1}{4}\Gamma\sin^2(2\theta)$, $\Gamma_{2\to1} = \Gamma\sin^4(\theta)$, and $\Gamma_{1\to2} = \Gamma\cos^4(\theta)$ from dressed-state levels linking neighbor manifolds (see Fig. 3). U describes the influence of the average phase shift on the evolution of the system under discussion.

Since we are interested in the conditions for the transition of coupled atom-light states to thermal equilibrium, we have introduced in Eqs. (16) the term $2wS_z^{(\rm eq)}/(2w + \Gamma_+)$ for the evolution of the Bloch vector component S_z. The presence of such a term in the set of Eqs. (16) is compatible with existing theories of spin-boson interaction with thermostat particles (due to collisions in our case) discussed by Leggett *et al.* in [28]. In particular, according to our approach in the ideal case, neglecting spontaneous emission terms in (16), the dressed-state population imbalance S_z should reach its thermodynamically equilibrium value $S_z^{(\rm eq)}$ with the rate $2w$ due to collisions with buffer gas atoms [see (21)], which is in agreement with experimentally tested approaches to OCs based on the solution of Boltzmann-like (rate) equations [11,26].

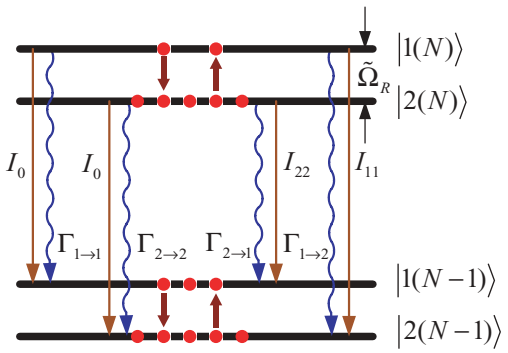

FIG. 3. (Color online) Energy (population) transfer between levels of the dressed atom induced by dephasing collisions. I_0, I_{11}, and I_{22} indicate intensity weights of three-color photon emission. In addition, spontaneous emission described by the rates $\Gamma_{i\to j}$ $(i,j=1,2)$ causes a transfer between levels of different manifolds.

The dependence of $S_z^{(\mathrm{eq})}$ on temperature can be easily understood from the thermodynamic properties of the coupled atom-light system (cf. [11], [29]). In particular, the population of the lower dressed state $|2(N)\rangle$ should be much larger [$\exp(\hbar\Omega_R/k_BT)$ times] than that of the upper one in thermal equilibrium. We suppose

$$S_z^{(\mathrm{eq})} = -\tanh\left(\hbar\Omega_R/2k_BT\right) \approx -\tanh\left(\hbar\,|\delta|\,/2k_BT\right), \qquad (18)$$

where the latter expression is valid under the perturbative limit (13). In particular, for a near-resonant atom-field interaction (when inequality $\hbar|\delta| \simeq \hbar\Omega_R \ll k_BT$ is still true), the equilibrium value of S_z according to Eq. (18) is $S_z^{(\mathrm{eq})} = 0$ and we arrive at the well-known result for which collisions with buffer gas atoms tend to equalize the population of the dressed states (cf. [12]).

In the opposite limit of large detuning, one can omit the terms containing collisional broadening γ and spontaneous emission Γ from Eqs. (16) and obtain the same results as in [29], obtained from the Schrödinger representation for OCs. In particular, without emission the collisions do not induce transitions between state $|a,N+1\rangle$ and state $|b,N\rangle$. Collisionally aided excitation allows a transfer between dressed-state components also in the case of large detunings. The energy difference is balanced by the kinetic energy of the colliding particles. Since state $|2(N)\rangle$ is energetically lower than state $|1(N)\rangle$, energy is taken from the thermal reservoir of the buffer gas during the transition from $|2(N)\rangle$ to $|1(N)\rangle$ (Fig. 2). About 10^3–10^4 collisions happen during the natural lifetime τ_{spont} of rubidium atoms.

The population transfer between dressed states evokes a thermalization process of coupled atom-light states which is characterized by the thermalization rate $2w = \gamma(\Omega_0^2/\Omega_R^2) \approx \gamma(\Omega_0^2/\delta^2)$ in Eq. (16c) for the dressed-state population imbalance S_z. Notably, $2w$ depends on the collisional rate γ as well as on the ratio Ω_0/δ, which characterizes the atom-field interaction. The dependence of $2w$ on the laser intensity is in agreement with present theories on OCs (see, e.g., [25]), whose validity in the yet unexplored high-pressure buffer gas regime with a high multiparticle collisional rate, however, remains to be tested.

IV. THERMALIZATION OF COUPLED ATOM-LIGHT STATES

Our goal in this section is to find stationary solutions of Eqs. (16) which are close to the thermodynamically true equilibrium state $S_z^{(\mathrm{eq})}$ of the coupled atom-field system. The full set of Eqs. (16) yields steady-state solutions:

$$S_x^{(\mathrm{st})} = -\frac{1}{D}\left[-\Gamma\sin 2\theta\left(\frac{\Gamma}{2}+\gamma\right)+2\left[U\tilde{\Omega}_R+(\alpha-\Gamma_{12})\left(\frac{\Gamma}{2}+\gamma\right)\right]\left(S_z^{(\mathrm{st})}-\frac{2wS_z^{(\mathrm{eq})}}{2w+\Gamma_+}\right)\right], \qquad (19a)$$

$$S_y^{(\mathrm{st})} = \frac{1}{D}\left[2[U(\Gamma_{\mathrm{coh}}+\varsigma)-\tilde{\Omega}_R(\alpha-\Gamma_{12})]\left(S_z^{(\mathrm{st})}-\frac{2wS_z^{(\mathrm{eq})}}{2w+\Gamma_+}\right)+\tilde{\Omega}_R\Gamma\sin 2\theta\right], \qquad (19b)$$

$$S_z^{(\mathrm{st})} = \frac{2wS_z^{(\mathrm{eq})}}{2w+\Gamma_+}+\frac{D\Gamma_- - 2\Gamma\sin 2\theta\left[(\alpha-\Gamma_{12})\left(\frac{\Gamma}{2}+\gamma\right)+U\tilde{\Omega}_R\right]}{(2w+\Gamma_+)D-4\left[2U\tilde{\Omega}_R(\alpha-\Gamma_{12})+(\alpha-\Gamma_{12})^2\left(\frac{\Gamma}{2}+\gamma\right)-U^2(\Gamma_{\mathrm{coh}}+\varsigma)\right]}, \qquad (19c)$$

where we made the denotation $D \equiv \tilde{\Omega}_R^2+(\Gamma_{\mathrm{coh}}+\varsigma)[(\Gamma/2)+\gamma]$.

First, we examine the role of atomic collisions in the thermalization process, completely neglecting spontaneous emission within the so-called secular approximation:

$$\Gamma \ll \gamma, \quad \eta \ll \Omega_R. \qquad (20)$$

In this case from expressions (19) one can assume that

$$S_x^{(\mathrm{st})} \approx S_y^{(\mathrm{st})} \approx 0, \qquad (21a)$$

$$S_z^{(\mathrm{st})} \approx S_z^{(\mathrm{eq})}. \qquad (21b)$$

The inequalities (20) represent the necessary condition for achieving a thermodynamically true equilibrium (21b) for the dressed-state population. The coupling between dressed-state coherences σ_{12} (σ_{21}) and populations σ_{11},σ_{22} can be completely neglected in this case; see (21a) (cf. [11]).

The thermodynamically full equilibrium behavior of the dressed-state population imbalance $S_z^{(\mathrm{eq})}$ is represented by the dotted (red) curve in Fig. 4. It is important to emphasize that the atomic ensemble under discussion indicates a two-level system without inversion under the perturbative limit (13) for negative atom-field detuning δ only. Actually in this limit from dressed-state definitions (9), we have $\sin\theta \simeq 0$,$\cos\theta \simeq 1$,

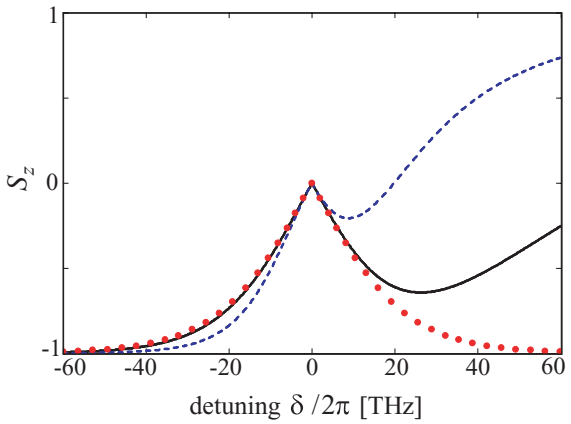

FIG. 4. (Color online) Dependence of dressed-state population imbalance S_z as a function of detuning $\delta/2\pi$ for 500-bar argon gas collisional broadening $\gamma/2\pi = 3.6$ THz; collisional shift $\eta/2\pi = -3$ THz. The resonant Rabi splitting frequency $\Omega_0/2\pi$ is infinite for the dotted (red) curve, 0.1 THz for the solid (black) curve, and 0.03 THz for the dashed (blue) curve. In all cases the gas temperature is $T = 530$ K and the spontaneous emission rate is $\Gamma \simeq 37$ MHz.

and the lower dressed state $|2(N)\rangle$, which is macroscopically occupied, corresponds to the bare state $|a,N+1\rangle$, which describes atoms in the ground state.

For large positive atom-light field detuning $\delta > 0$ under condition (13), we can put $\sin\theta \simeq 1$, $\cos\theta \simeq 0$, in Eqs. (9), which implies that the lower dressed state $|2(N)\rangle$ corresponds to the excited atomic level $|b,N\rangle$, which is much more populated. In this case we achieve inversion in the two-level atomic system under thermal equilibrium (cf. [29]).

The decay of atomic upper level $|b\rangle$ with the rate Γ leads to nonequilibrium processes in the dressed-state population behavior. Taking into account (16c) spontaneous emission under the assumption (21a), we get a steady-state solution for the dressed-state population imbalance S_z:

$$S_z = \frac{2w(\theta)S_z^{(\mathrm{eq})} + \Gamma_-(\theta)}{2w(\theta) + \Gamma_+(\theta)}. \tag{22}$$

In Fig. 4 the dependence of the dressed-state population imbalance S_z in the steady state (22) on the atom-field detuning δ is plotted. The full thermalization of the atom-light state (dotted curve in Fig. 4) is approached at infinite Rabi frequency (i.e., for infinite input laser power) only. The same result can be obtained from Boltzmann-like (rate) equations for dressed-state populations if the contribution from spontaneous emission to the thermalization of the atom-field states is completely neglected (cf. [11]). The asymptotic behavior of population imbalance presented in Fig. 4 for large values of atom-field detuning δ can be easily analyzed in the perturbative limit (13) under condition (12). In particular, from (22) one can obtain

$$S_z \approx S_z^{(\mathrm{eq})} + \frac{\frac{\Omega_0^4}{8\delta^4} - 2e^{-\hbar|\delta|/k_BT}}{1 + \frac{\gamma\Omega_0^2}{\Gamma\delta^2}} \quad \text{for} \quad \delta < 0, \tag{23a}$$

$$S_z \approx S_z^{(\mathrm{eq})} + \frac{2}{1 + \frac{\gamma\Omega_0^2}{\Gamma\delta^2}} \quad \text{for} \quad \delta > 0. \tag{23b}$$

The terms containing Γ in (22) and (23) characterize the influence of spontaneous emission on the thermalization process. The decay of the dressed-state population imbalance in (22) due to spontaneous emission is described by Γ_+. To minimize this effect we require the rate of thermalization of atom-field dressed state $2w$ to be much higher than the effective rate of spontaneous emission Γ_+; that is, the inequality

$$2w \gg \Gamma_+ \tag{24}$$

should be satisfied.

With the help of definitions (17) and (24), one can obtain

$$\frac{\Gamma}{\gamma} \ll \frac{\Omega_0^2}{\delta^2} \ll 1. \tag{25}$$

Relation (25) is one of the main results of the paper and a characterizing condition for reaching true thermal equilibrium of coupled atom-field (dressed) states. Such an equilibration is achieved at the far detuned tails of dressed-state population imbalance S_z in Fig. 4, for which, with condition (23), we have $S_z \approx S_z^{(\mathrm{eq})}$.

The suppression of the thermalization process due to spontaneous emission leads to the formation of thermodynamically quasiequilibrium of coupled atom-light states for which condition (25) is violated. Indeed, for

$$\frac{\Omega_0^2}{\delta^2} \ll \frac{\Gamma}{\gamma} \ll 1, \tag{26}$$

from (23) we get

$$S_z \approx S_z^{(\mathrm{eq})} + \frac{\Omega_0^4}{8\delta^4} - 2e^{-\hbar|\delta|/k_BT} \quad \text{for} \quad \delta < 0, \tag{27a}$$

$$S_z \approx S_z^{(\mathrm{eq})} + 2 \quad \text{for} \quad \delta > 0. \tag{27b}$$

For highly nonequilibrium coupled atom-light states $S_z \approx 1$ [see (27b) and Fig. 4] and spontaneous emission decay drives the dressed-state system out of equilibrium for large positive detuning δ. In conclusion, Eqs. (16) yield a stationary solution only.

Conditions (24) and (25) can be represented in some other form introducing the time of thermalization T_{therm} of coupled atom-field states as follows:

$$T_{\mathrm{therm}} \equiv \frac{2\pi}{2w} = \frac{2\pi}{\gamma}\left(1 + \frac{\delta^2}{\Omega_0^2}\right). \tag{28}$$

According to this definition the minimal time of thermalization $T_{\mathrm{therm}}^{(\mathrm{min})} \simeq 2\pi/\gamma$ occurs for a near-resonant atom-field interaction ($|\delta| \ll \Omega_0$) representing state (1) in Fig. 2. The time $T_{\mathrm{therm}}^{(\mathrm{min})}$ is in the picosecond regime for experimentally accessible collisional broadening γ.

For large atom-light detuning in the perturbative limit (13), the time of thermalization T_{therm} increases and approaches

$$T_{\mathrm{therm}} \approx \frac{2\pi\delta^2}{\gamma\Omega_0^2} \simeq \frac{2\pi k_B^2 T^2}{\gamma\hbar^2\Omega_0^2}. \tag{29}$$

Notably, the quantity T_{therm} is inversely proportional to Ω_0^2, that is, to the incident optical power P_0. Taking into account definition (28), we can express condition (24) for thermalization of atom-field coupled states as

$$T_{\mathrm{therm}} \ll \tau_{\mathrm{spont}}. \tag{30}$$

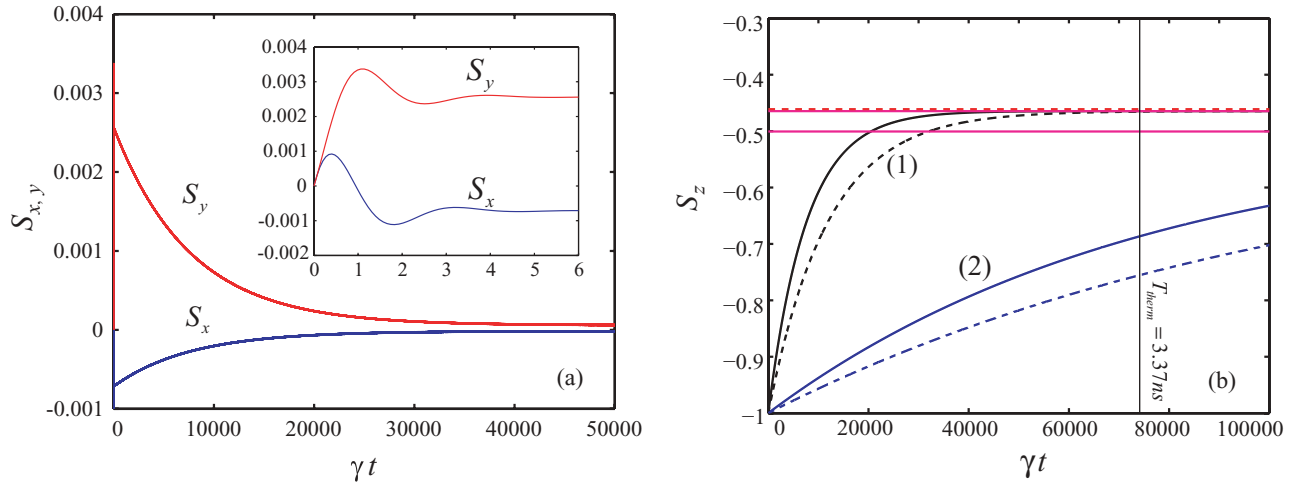

FIG. 5. (Color online) Dependences of (a) dressed-state pseudospin components $S_{x,y}$ and (b) population imbalance S_z as a function of reduced time γt. Parameters are $\gamma/2\pi = 3.6$ THz, $\eta/2\pi = -3$ THz, $\Gamma \simeq 37$ MHz, $\delta/2\pi = -11$ THz, and $T = 530$ K. The resonant Rabi splitting frequency $\Omega_0/2\pi$ is 0.1 THz for curves (1) and 0.03 THz for curves (2). Initial conditions are $S_{x,y}(0) = 0$ and $S_z(0) = -1$. The vertical line corresponds to the time $T_{\rm therm}$ of thermalization of coupled atom-light states for $\Omega_0/2\pi = 0.1$ THz.

Thereby, at appropriate time scales the thermalization time $T_{\rm therm}$ of the atom-field dressed states must be faster than the atomic transition lifetime $\tau_{\rm spont}$. In particular, for our experiment the minimal achievable time of thermalization at full optical power is about 3.37 ns for argon buffer gas and 10.8 ns for helium (see Sec. VI).

Now let us examine nonequilibrium properties of the atom-light states. The value of detuning δ is of the order of the collisional broadening γ in our experiment. In fact, we are working beyond the secular approximation limit established by (20). In this case the Bloch components S_x and S_y can be adiabatically eliminated from Eqs. (16) and we can obtain the following solution for the dressed-state population imbalance S_z:

$$S_z(t) = S_z^{(\rm st)} + \left[S_z(0) - S_z^{(\rm st)}\right] e^{-(2w+\Gamma_+)t}, \qquad (31)$$

where $S_z(0)$ is the initial value of the pseudospin component S_z at $t = 0$, and $S_z^{(\rm st)}$ is determined by Eq. (19c).

The numerical solution of the full set of Eqs. (16) revealing the quasiequilibrium dynamics of the coupled atom-light system for 500-bar argon buffer gas is presented in Fig. 5. We suppose that all atoms initially occupy the lower dressed-state level $|2(N)\rangle$; that is, $S_z(t = 0) = -1$. Figure 5(a) demonstrates the decreasing atomic polarization described by dressed-state coherences, the Bloch vector components S_x and S_y, respectively. In particular, in the steady-state $S_{x,y}$ tend to the values $S_{x,y}^{(\rm st)}$ according to Eqs. (19a) and (19b). They clearly exhibit the presence of some small (residual) polarization of the atomic medium which depends on the vital parameter Γ_+/w. The dressed-state coherences S_x and S_y are relatively large for nonequilibrium states when $\Gamma_+ \gg w$. On the contrary, we can use Eq. (21a) and ignore the dressed-state polarization at full thermal equilibrium under the secular approximation (20).

The transient regime of thermalization of coupled atom-light states for the experiment described in Sec. VI is presented in Fig. 5(b). The dependences based on a numerical solution of full Eqs. (16) are represented by solid curves in Fig. 5(b). Dashed curves correspond to expression (31). The steady-state levels for various resonant Rabi frequencies $\Omega_0/2\pi$ are shown by horizontal (magenta) lines. These levels are determined by the magnitude of population imbalance S_z for a detuning $|\delta| = k_B T/\hbar$ that corresponds to a frequency of about 11 THz. From Fig. 5(b) it follows that for sufficiently long time scales such as $t \gg 1/(2w + \Gamma_+)$, the dressed-state population imbalance $S_z(t)$ reaches its steady-state value $S_z^{(\rm st)}$ (for a given Rabi frequency $\Omega_0/2\pi$) as determined by expression (19c).

V. INTENSITIES OF SPECTRAL COMPONENTS

Here we discuss the modification of the intensities of the fluorescence spectrum components under the thermalization of atomic dressed states. In general the fluorescence triplet consists of a central line of frequency ω_L and two sidebands centered at $\omega_L \pm \Omega_R$ (see Fig. 3). These lines have intensities with weights

$$I_{11} \equiv I(\omega_L + \Omega_R) = \sigma_{11}\Gamma_{1\to 2} = \Gamma \cos^4(\theta)\frac{w(\theta)\left[1 + S_z^{(\rm eq)}\right] + \Gamma \sin^4\theta}{2w(\theta) + \Gamma_+(\theta)}, \qquad (32a)$$

$$I_{22} \equiv I(\omega_L - \Omega_R) = \sigma_{22}\Gamma_{2\to 1} = \Gamma \sin^4(\theta)\frac{w(\theta)\left[1 - S_z^{(\rm eq)}\right] + \Gamma \cos^4\theta}{2w(\theta) + \Gamma_+(\theta)}, \qquad (32b)$$

$$I_0 \equiv I(\omega_L) = \Gamma \sin^2(\theta)\cos^2(\theta). \qquad (32c)$$

Following (32c) the I_0 intensity component weight is still unchanged during the thermalization process because it does not depend on temperature. In other words, thermalization of coupled atom-light states reduces to redistribution of intensities between the I_{11} and the I_{22} components.

To be more specific, we examine Eqs. (32) in the perturbative limit (13) for negative detuning $\delta < 0$. In this case we can assume that $\sin^2(\theta) \approx \Omega_0^2/4\delta^2$, $\cos^2(\theta) \approx 1$ [see (11)]. At the same time in this limit we have $|1(N)\rangle \sim |b, N\rangle$

and $|2(N-1)\rangle \sim |a,N\rangle$ for dressed levels of one manifold. Physically this means that I_{11} approximately corresponds to the transition from the upper to the lower state (see Fig. 3).

Let us now analyze Eqs. (32) in the limit where thermalization does not occur, that is, when condition (26) is fulfilled for coupled atom-light states. From (32) we get

$$I_{11} \approx w\left(1+S_z^{(\mathrm{eq})}\right) \approx \frac{\gamma\Omega_0^2 e^{-\hbar|\delta|/k_BT}}{\delta^2}, \tag{33a}$$

$$I_{22} \approx \frac{\Gamma\Omega_0^4}{16\delta^4}, \tag{33b}$$

$$I_0 = \frac{\Gamma\Omega_0^2}{4\delta^2}. \tag{33c}$$

In expressions (33) we arrive at familiar results (see, e.g., [12]) in the limit of near-resonant atom-field interaction when $\hbar|\delta| \ll k_BT$ and $I_{11} \approx 2I_0\gamma/\Gamma \gg I_0$. However, in the general case, from (33) we obtain

$$\frac{I_{11}}{I_0} \approx \frac{4\gamma e^{-\hbar|\delta|/k_BT}}{\Gamma}. \tag{34}$$

For large detuning δ, one can have $I_{11} \ll I_0$ under the condition $\hbar|\delta| \gg k_BT\ln[4\gamma/\Gamma]$. However, such a condition is not realized for the experimentally accessible range of detuning δ and temperatures T – cf. (12).

We can show that in the presence of thermal equilibrium, under conditions (24) and (25) the I_{11} intensity component changes essentially, and from (32a) we obtain

$$I_{11}^{(\mathrm{therm})} \approx \Gamma e^{-\hbar|\delta|/k_BT}. \tag{35}$$

At the same time the other intensity weights, I_{22} and I_0, still remain unchanged [see Eqs. (33b) and (33c)]. From (33a) and (35) it is easy to see that

$$I_{11} \ll I_{11}^{(\mathrm{therm})}, \tag{36}$$

which implies a significant increase in I_{11} under the thermalization process.

Now let us turn our attention to positive-valued large atom-field detuning, that is, to $\delta > 0$. Without thermalization ($2w \ll \Gamma$), from (32a) and (32b) we get [cf. (33a) and (33b)]:

$$I_{11} \approx \frac{\Gamma\Omega_0^4}{16\delta^4}, \tag{37a}$$

$$I_{22} \approx \frac{\gamma\Omega_0^2}{\delta^2}. \tag{37b}$$

On the contrary, Eqs. (32a) and (32b) approach

$$I_{11}^{(\mathrm{therm})} \approx \frac{\Gamma\Omega_0^4}{16\delta^4} e^{-\hbar|\delta|/k_BT}, \tag{38a}$$

$$I_{22}^{(\mathrm{therm})} \approx \Gamma, \tag{38b}$$

under the fulfillment of conditions (24) and (25).

Thus, thermalization of coupled atom-light states for positive detuning δ is mostly due to the dramatic increase in the I_{22} intensity weight component and suppression of the I_{11} component simultaneously.

It is also fruitful to introduce the total intensity weight of fluorescence (absorption) I as a sum of all intensity weights

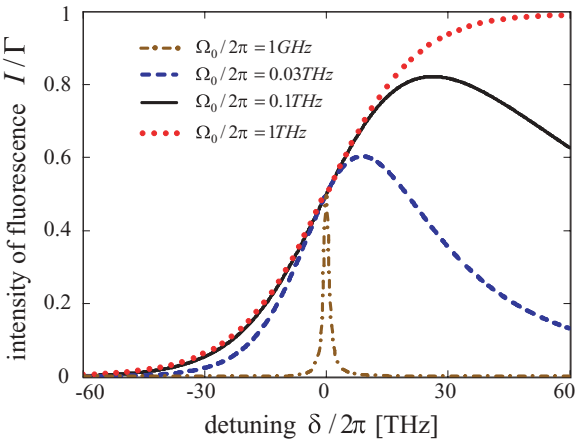

FIG. 6. (Color online) The reduced intensity of fluorescence I versus atom-field detuning $\delta/2\pi$ for 500-bar argon buffer gas at different values of the resonant Rabi frequency $\Omega_0/2\pi$.

represented in (32); that is, $I = I_{11} + I_{22} + I_0$. With the help of definitions (9) and (14), from (32) we get

$$I = \sigma_{bb}\Gamma = \frac{\Gamma}{2}\left(1 - \frac{\Gamma\cos^2(2\theta)}{2w+\Gamma_+}\right) + \frac{\Gamma w\cos(2\theta)\, S_z^{(\mathrm{eq})}}{2w+\Gamma_+}, \tag{39}$$

where $\sigma_{bb} = \langle b,N|\sigma|b,N\rangle$ is the population of the upper (excited) atomic state.

The thermalization of the atom-light field states is determined by the last term in (39) (cf. [12]). In Fig. 6 the dependence of the reduced intensity weight I/Γ (excited atomic-state population σ_{bb}) is presented as a function of atom-light field detuning δ. The asymmetry of the behavior of I in Fig. 6 can be easily understood by introducing the difference ΔI between positive (far blue wing)- and negative (far red wing)-valued detuning intensities for which, from (39), we obtain

$$\Delta I \equiv I(\delta>0) - I(\delta<0) \approx \frac{2\Gamma w\tanh(\hbar|\delta|/2k_BT)}{2w+\Gamma_+}. \tag{40}$$

For complete thermalization of the atom-field states [dotted (red) curve in Fig. 6], under condition (25) the intensity weight of fluorescence I can be approximated by a Fermi-Dirac distribution function as

$$I \simeq \frac{\Gamma}{1+e^{-\hbar\delta/k_BT}}. \tag{41}$$

In this limit the maximal intensity weight is $I^{(\mathrm{therm})} \approx \Gamma$ (for $\delta > 0$) and ΔI approaches

$$\Delta I^{(\mathrm{therm})} \simeq \Gamma\ \tanh(\hbar|\delta|/2k_BT) \approx \Gamma. \tag{42}$$

On the contrary, for small Rabi frequencies (curves describing nonequilibrium states in Fig. 6), from (40) we have

$$\Delta I \approx \frac{\gamma\Omega_0^2}{\delta^2}\tanh(\hbar|\delta|/2k_BT) \ll \Gamma, \tag{43}$$

which implies fulfillment of condition $\Delta I \ll \Delta I^{(\mathrm{therm})}$ [cf. (36)].

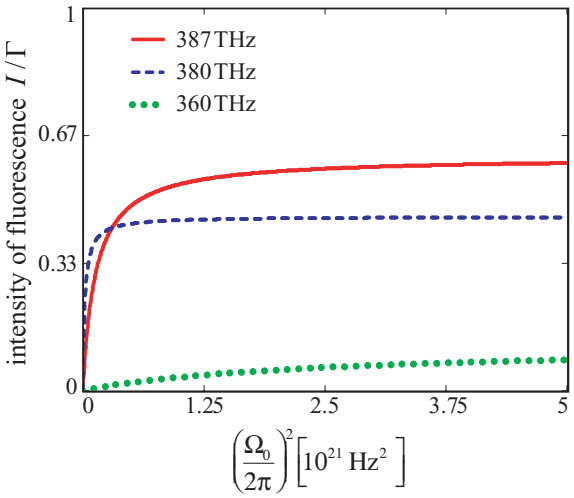

FIG. 7. (Color online) The reduced intensity of fluorescence I versus the square of the resonant Rabi frequency for 400-bar helium buffer gas at three different frequencies of the laser field.

In Fig. 7 calculated dependencies of the total normalized intensity weight I versus the square of the resonant Rabi frequency (as a measure of the intensity) are presented. Physically, they reflect the fact that the population of the atomic ground state $|a\rangle$ decreases, while that of the upper level (population σ_{bb}) increases, with increases in the incident optical power, that is proportional to the square of resonant Rabi frequency Ω_0 [cf. (39)].

To end the theoretical part of the paper, let us briefly discuss the boundaries of applicability of our theoretical model for OCs. It is necessary to accentuate the impact limit ($\Omega_R \tau_{\mathrm{coll}} \ll 1$) of OCs when the processes of Rabi oscillations, spontaneous emission, and atomic collisions are mutually uncorrelated. Only in this case is the master Eq. (2) used in this paper valid. In our experiment the impact limit is not completely fulfilled (see Sec. VI). In particular, only inequality $\Omega_0 \ll \tau_{\mathrm{coll}}^{-1}$ takes place in our case. At the same time the experimentally accessible atom-light detuning δ is of the order of the inverse time of collisions $\tau_{\mathrm{coll}}^{-1}$.

Further, we do not take into account the influence of the Franck-Condon factor (overlapping integral) in electric dipole operators, which characterizes overlapping between the (quasi-) molecular wave functions for initial and final states during the collision (see, e.g., [30]). Obviously, this factor becomes more important when the impact limit breaks down (for detuning δ such as $|\delta|\tau_{\mathrm{coll}} \gg 1$) and a full quantum mechanical approach to OCs and line profile description become necessary (cf. [18], [31], [32]). Nevertheless, as we will see, the dependences in Figs. 6 and 7, obtained under the proposed theoretical approach, are qualitatively in good agreement with obtained experimental results.

VI. EXPERIMENT: THERMAL EQUILIBRIUM FOR COUPLED ATOM-LIGHT STATES

We now proceed to experimental work, in which we have investigated rubidium atoms under an extraordinarily high buffer gas pressure driven by tunable laser radiation. The aim of our work presently is to reach thermal equilibrium

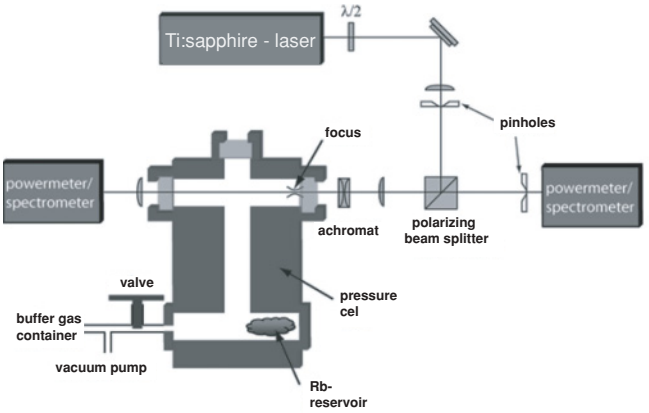

FIG. 8. Experimental setup.

of coupled atom-light states. Clearly, thermal equilibrium is a prerequisite for observation of a Bose-Einstein-like phase transition for polaritons. The large collisional broadening in our system interpolates between the usual atomic gas phase and the solid or liquid phase condition.

A. Experimental setup

A scheme of our experimental setup used to investigate atom-light interaction at ultrahigh buffer gas pressures and intense laser radiation is shown in Fig. 8. A stainless-steel high-pressure cell filled with atomic rubidium is used, which is connected by a valve to a buffer gas reservoir. Alternatively helium or argon buffer gas at pressures up to 230 bar is filled into the cell at room temperature. By heating the sealed cell up to 530 K, a buffer gas pressure of 500 bar for argon and a rubidium density of 10^{16} cm^{-3} are reached. Tunable laser radiation derived from a titanium-sapphire laser tuned to the rubidium D lines is focused on the cell to a waist size of 3 μm. The focus is placed directly behind the window to suppress propagation effects. To detect fluorescence light selectively from the focal region, where high laser intensities, up to 10^9 mW/cm^2, for an optical power of 300 mW are reached, both the incident beam and the outgoing fluorescence are spatially filtered with pinholes in a confocal geometry.

B. Excited-state lifetime measurements

In initial experiments, we have measured the lifetime of the rubidium $5P$ excited state in the presence of high buffer gas pressures. The lifetime of excited states is a major limitation of the coherence time in semiconductor polariton BEC experiments, which is here typically close to 1 ps [1]. For the excited-state lifetime measurement in our rubidium high-pressure buffer gas system, we have chopped the exiting Ti:sapphire laser beam with an acousto-optical modulator (not shown in Fig. 8) and measured the fluorescence in the backward direction with a photomultiplier. Measurements of the $5P$-$5S$ fluorescence decay time for various buffer gas pressures of argon and helium are shown in Fig. 9. For low pressures the decay time is significantly longer than the natural $5P$ lifetime of 27 ns [27]. We ascribe the slow decay of the fluorescence signal to energy pooling [33], where in excited-atom/excited-atom collisions two Rb atoms pool their

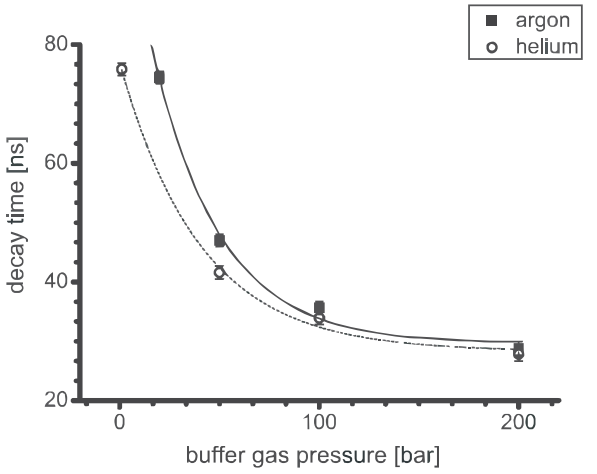

FIG. 9. Observed fluorescence decay time of the 5*P* rubidium excited state versus buffer gas pressure. Data recorded for argon (squares) and helium (circles) gas, together with exponential decay curves fitted to the data for helium (dashed line) and for argon (solid line).

internal energy to produce one ground-state atom and one in a higher excited state. A highly excited atom with a long lifetime can subsequently decay into the 5*P* state. Therefore energy pooling yields a reoccupation process of the 5*P* state that increases the observed 5*P*-5*S* fluorescence decay time. For higher buffer gas pressures the observed decay time is reduced and tends to approach the expected 5*P* natural lifetime. We attribute this to a decline in the energy pooling process that involves highly excited rubidium states at high buffer gas pressures, which reduces the efficiency of the repopulation process at high pressure values. This interpretation of the measured decay times is supported by the observed strong blue fluorescence near 420 nm, which gives clear evidence of the presence of energy pooling, at low buffer gas pressures. Further, with increasing pressure the intensity of the blue fluorescence decreases considerably.

To guide the eye, exponential decay curves have been fitted to the lifetime measurement data. The graphs approach a decay time of 28.3 ± 1.9 ns for helium and 29.6 ± 2.2 ns for argon at high pressure values. These values would coincide with the natural lifetime within our experimental accuracy.

No evidence of a decline in the 5*P* lifetime, possibly to quenching, was observed within our present measurement accuracy up to the quoted pressure value of 200 bar, which was the maximum available buffer gas pressure in these data sets. In future, we plan to extend these lifetime measurements toward higher buffer gas pressures.

C. Measurements indicating thermal quasiequilibrium of atom-light states

In subsequent measurements we have recorded spectra of the rubidium *D* lines at ultrahigh buffer gas pressures. Typical fluorescence spectra recorded at 530 K and 400 bar helium buffer gas pressure for variable optical powers are shown in Fig. 10(a). Since the fluorescence is measured in the experiment, the population of dressed states and population of excited atomic level σ_{bb} [see (39)] are of interest as well.

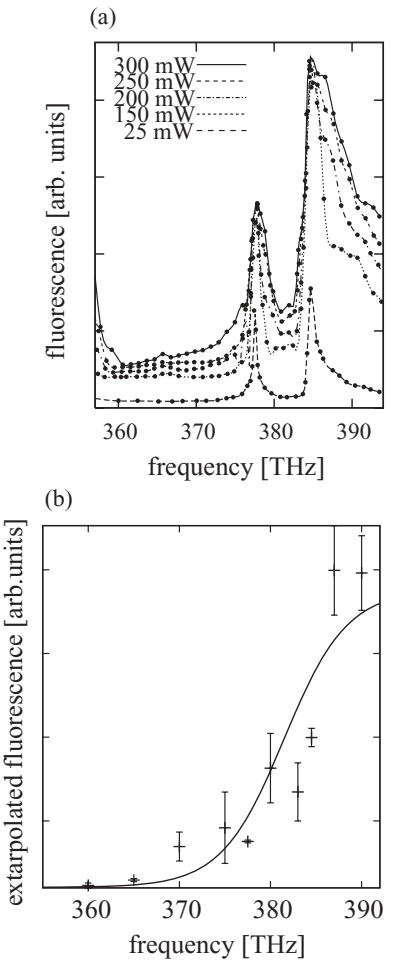

FIG. 10. (a) Rubidium fluorescence signal and (b) results of extrapolation of measurement data to infinite laser intensity as a function of the incident frequency: both for helium buffer gas. Error bars were obtained from extrapolation fits. Data were fitted with a Fermi-Dirac distribution, assuming thermal equilibrium of the two-level dressed-state system [cf. (41)].

At a moderate optical power ($P = 25$ mW) the usual pressure-broadened rubidium D_1 and D_2 lines are visible. The resonant Rabi frequency $\Omega_0/2\pi$ is about 0.03 THz in this case, and we deal with state (3), which is placed far from the region of the resonant atom-field interaction (see Fig. 2). For atom-field detuning $\delta/2\pi = -11$ THz and for collisional broadening $\gamma_{\mathrm{Ar}}/2\pi \simeq 3.6$ THz, the minimal thermalization time occurs for a 500-bar argon buffer gas pressure and $T_{\mathrm{therm}} \approx 37.4$ ns in this case, which is of the order of spontaneous emission lifetime $\tau_{\mathrm{spont}} = 27$ ns. Thus, we have not yet reached thermal equilibrium for such a state, represented by dashed (blue) curves in Figs. 4 and 5.

In particular, at the experimentally achieved maximal power $P \simeq 300$ mW, the resonant Rabi frequency is $\Omega_0/2\pi \simeq 0.1$ THz and the time of thermalization T_{therm} approaches 10.8 ns (for 400-bar helium buffer gas pressure) and 3.37 ns (for 500-bar argon buffer gas pressure). The latter value is essentially shorter than the spontaneous emission lifetime τ_{spont}. In this sense we can speak about achieving equilibrium for coupled atom-light states [state (2) in Fig. 2] in the experiment (see Fig. 5).

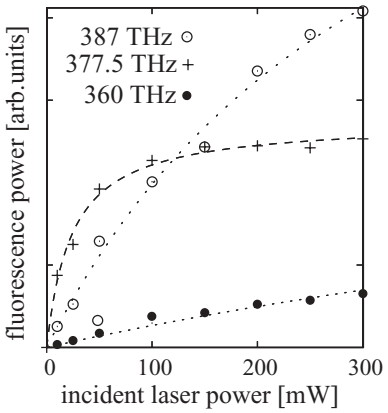

FIG. 11. Fluorescence signal at 400-bar helium buffer gas as a function of input laser power for three different values of laser frequency.

Further diminishment of the thermalization time is possible by increasing the incident optical power. Notably, full thermalization of the coupled atom-light state is achieved for infinite laser power (cf. Fig. 4) or full line saturation (see Fig. 11).

For the purpose of comparison the expected fluorescence signal at full saturation versus frequency is shown in Fig. 10(b). It was derived at each frequency point by extrapolating the observed fluorescence to infinite laser intensity. Interestingly, this spectrum of the extrapolated fluorescence can be fitted well by a Fermi-Dirac function $I(\delta)$ (solid line) [see (41)]. We interpret these measurements as evidence for approach of dressed-state thermal equilibrium at high drive laser powers (cf. Fig. 6). Strictly speaking, only in this case does the Franck-Condon factor (overlapping of quasimolecular wave functions) not matter.

Figure 11 shows the experimentally observed fluorescence versus optical power for three different laser frequencies for the helium buffer gas data. Near a line center (crosses) the curve has already saturated at a relatively low power level to an intermediate fluorescence level. For significant detuning, the optical power at which saturation is achieved is higher, as visible for both blue (open circles) and red (filled dots) detunings.

Interestingly, the saturation level of fluorescence is clearly different in both cases, with the blue (red) detuning leading to the largest (smallest) values. At full saturation, where spontaneous processes are negligible compared to stimulated processes, we expect the dressed-state populations to be in full thermal equilibrium (cf. Figs. 4 and 7).

During the course of the experiments, we found that the results of the spectral measurements were critically dependent on the purity of the buffer gas used and presumably, also, the decomposition of residual impurities. The measurements shown in Fig. 10 were carried out using the buffer gas argon/helium 5.0 (supplier, Air Liquide). In contrast, we did not observe significant saturation of the fluorescence at high laser powers for buffer gas from a different supplier (argon/helium 5.0; supplier, Praxair). We attribute this to different residual impurity compositions. In a pure inert buffer gas system this perturbation apparently does not occur at a significant rate, which reveals the remarkable elasticity of alkali gas atoms in collisions with inert gas atoms. To experimentally reach full thermal equilibrium also at very large laser detuning, it is necessary to enlarge the coupling in the atom-light system. This can be achieved by use of a higher laser power or a cavity-based system.

D. Toward thermalization of atom-light states with a continuum of modes

Up to now thermal equilibrium of a coupled atom-light system has been investigated for the case of a two-level dressed-state system. The observation of a Bose-Einstein-like phase transition from a thermal state to an ordered polariton state, however, requires a continuum of modes (see, e.g., [34–36]), as, for example, provided by the transverse modes of an optical cavity. Alternatively, a suitable optical waveguide could be used. To allow accumulation of polariton modes at the lowest available energy, it is clear that a process must exist that allows a continuous change of photon wavelengths toward lower energies, at least in the region around the lowest available photon energy of the optical resonator.

In our rubidium high-pressure buffer gas system, we have tested for the presence of such frequency shifting processes. For this experiment, we spectrally analyzed the radiation detected at the cell output in the forward direction behind a second window of the cell (see Fig. 8). Note that in this forward-direction measurement, because of the comparatively long optical path through the cell (5 cm), the confocal parameter used ($\simeq$70 μm) is much shorter than the interaction length, so that the beam diameter increases considerably at the end of the cell and the optical intensity there is comparatively low. Due to the long interaction length, we also expect propagation effects to play a role. Typical spectra, measured with a grating spectrometer, are shown in Fig. 12 for various cell temperatures. The incident laser wavelength here was 790 nm, that is, between the rubidium D_1 and the rubidium D_2 lines. At moderate temperatures (200°C) the observed fluorescence spectrum covers the spectral range from 750 to 950 nm, with clear dips near the rubidium D lines, which we attribute to the greater absorption there. At higher temperatures and therefore higher Rb densities, the cell becomes optically

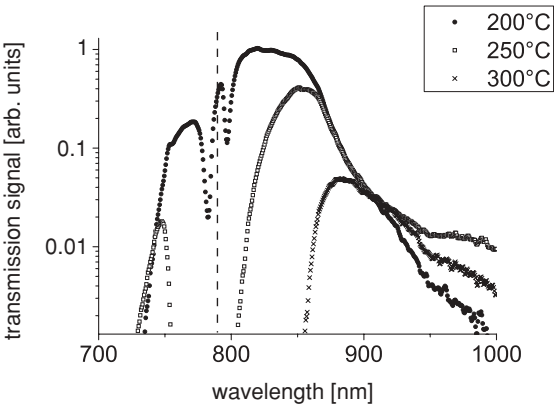

FIG. 12. Relative optical intensity measured in the forward direction after the cell versus frequency for different cell temperatures. The value of the incident laser wavelength (790 nm) is indicated by the dashed vertical line.

thick over a large spectral range near the rubidium resonances, and in this wavelength range little transmitted optical power is observed. The spectra show a broad fluorescence peak with a maximum wavelength exceeding 900 nm. The fluorescence signal observed at the cell output has maximum spectral intensity on the red side of the rubidium spectrum; that is, Stokes scattering is clearly stronger than anti-Stokes processes. We interpret the results of these measurements as evidence that processes exist which could support thermalization of photonic modes also in the case of a continuous mode spectrum, as required for experimental observation of a BEC-like phase transition of polaritons. Clearly, the efficiency of these wavelength shifting processes, and also thermalization of polariton modes, needs to be studied in detail in future work. For the rubidium buffer gas system, a reasonable choice of wavelength for the lowest-cavity mode seems to be between 800 and 900 nm, where optical modes are populated by Stokes scattering. The presence of the phase transition would change the broad fluorescence signal in the forward direction to a sharp peak located at the frequency of the lowest mode.

VII. CONCLUSIONS AND OUTLOOK

In this paper have we studied the thermalization of coupled atom-light states under the influence of OCs. We found that thermal equilibrium is possible by controlling the resonant Rabi frequency and the atom-light detuning. We have shown that a nonvanishing macroscopic polarization of the atomic medium occurs when the problem is described without the secular approximation, which is typically used in the problem under discussion. Experimentally we find evidence for a thermalization of the dressed atom-light states in an ultrahigh-pressure buffer gas environment. The observed intensity-dependent asymmetry of the spectra is interpreted as partial thermal equilibrium of dressed atom-light states, when the driving-field detuning is chosen as $|\delta| \simeq k_B T/\hbar$. The thermalization process results in significant energy redistribution within the two sideband intensity components. We have observed Stokes scattering and characterized the lifetime of excitations in the presence of the buffer gas.

In future, it will be important to add a spatial confinement to allow dispersion of the coupled atom-light eigenstates with a low-frequency cutoff, suitable for BEC. This can be implemented using either a resonator or a a waveguide structure. This also yields an enhancement of the field amplitude, which can allow full thermalization of coupled atom-light states in the high-pressure buffer gas system. When the rubidium density is increased, a strong coupling limit should be achievable in the buffer gas system, making polaritons relevant atom-light excitations. On the theoretical side it will be important to extend the treatment of coupled atom-light state (polariton) thermalization in the presence of OCs, as done in the present work.

We conclude that the ultrahigh-pressure buffer gas approach is a promising candidate for possible realization of a BEC-like phase transition of polaritons in an atomic physics system.

ACKNOWLEDGMENTS

This work was partially supported by Russian Foundation for Basic Research Grant No. 09-02-91350 and by the Deutsche Forschungsgemeinschaft within FOR 557 and cooperation project 436 RUS 113/996/0-1. We are grateful to the referees for their comments and the referral to the valuable Ref. [18]. A. P. Alodjants acknowledges financial support from Russian Federal Agency of Education under the program "Scientific and scientific-pedagogical potential of Russia for innovation".

[1] J. Kasprzak *et al.*, Nature **443**, 409 (2006).
[2] S. Utsunomiya *et al.*, Nature Phys. **4**, 700 (2008).
[3] M. Aichhorn, M. Hohenadler, Ch. Tahan, and P. B. Littlewood, Phys. Rev. Lett. **100**, 216401 (2008).
[4] A. Amo *et al.*, Nature **457**, 291 (2009).
[5] Ch. Bolkart, R. Weiss, D. Rostohar, and M. Weitz, Laser Phys. **15**, 3 (2005).
[6] V. A. Averchenko *et al.*, Rus. J. Quantum Electron. **36**, 532 (2006).
[7] M. J. Hartmann, F. G. S. L. Brandao, and M. B. Plenio, Nature Phys. **2**, 849 (2006).
[8] M. Fleischhauer, J. Otterbach, and R. G. Unanyan, Phys. Rev. Lett. **101**, 163601 (2008).
[9] D. Snoke and A. Kavokin, Solid State Commun. **144**, 357 (2007).
[10] H. Deng, D. Press, S. Gotzinger, G. S. Solomon, R. Hey, K. H. Ploog, and Y. Yamamoto, Phys. Rev. Lett. **97**, 146402 (2006).
[11] U. Vogl and M. Weitz, Phys. Rev. A **78**, 011401(R) (2008).
[12] C. Cohen-Tannoudji, J. Dupont-Roc, and G. Grynberg, *Atom-Photon Interactions: Basic Processes and Applications* (Wiley, New York, 1998).
[13] U. Vogl and M. Weitz, Nature **461**, 70 (2009).
[14] V. Weisskopf, Phys. Z. **34**, 1 (1933).
[15] A. Jablonski, Phys. Rev. **68**, 78 (1945); P. W. Anderson, *ibid.* **76**, 647 (1949); H. M. Foley, *ibid.* **69**, 616 (1946).
[16] S. Chen and M. Takeo, Rev. Mod. Phys. **29**, 20 (1957).
[17] M. Baranger, Phys. Rev. **111**, 481 (1958).
[18] A. Royer, Can. J. Phys. **52**, 1816 (1974); Phys. Rev. A **22**, 1625 (1980).
[19] N. Allard and J. Kielkopf, Rev. Mod. Phys. **54**, 1103 (1982).
[20] L. I. Gudzenko and S. I. Yakovlenko, Zh. Eksp. Teor. Fiz. **62**, 1686 (1972) [Sov. Phys. JETP **35**, 877 (1972)]; V. S. Lisitsa and S. I. Yakovlenko, Zh. Eksp. Teor. Fiz. **66**, 1550 (1974) [Sov. Phys. JETP **39**, 759 (1974)].
[21] S. Yeh and P. R. Berman, Phys. Rev. A **19**, 1106 (1979).
[22] R. E. M. Hedges, D. L. Drummond, and A. Gallagher, Phys. Rev. A **6**, 1519 (1972).
[23] C. Brechignac, Ph. Cahuzac, and P. E. Toschek, Phys. Rev. A **21**, 1969 (1980).
[24] J. L. Carlsten, A. Szoke, and M. G. Raymer, Phys. Rev. A **15**, 1029 (1977).
[25] S. I. Yakovlenko, Usp. Fiz. Nauk **136**, 593 (1982) [Sov. Phys. Usp. **25**, 216 (1982)].
[26] R. V. Markov, A. I. Plekhanov, and A. M. Shalagin, Phys. Rev. Lett. **88**, 213601 (2002).

[27] D. A. Steck, Rubidium 87 D line data; [http://steck.us/alkalidata] (2003).
[28] A. J. Leggett *et al.*, Rev. Mod. Phys. **59**, 1 (1987).
[29] R. V. Markov, A. I. Plekhanov, and A. M. Shalagin, Sov. JETP **93**, 1028 (2001).
[30] B. H. Bransden and C. J. Joachain, *Physics of Atoms and Molecules* (Longman Scientific & Technical, New York, 1990).
[31] N. F. Allard and F. Spiegelman, Astron. Astrophys. **452**, 351 (2006).
[32] N. F. Allard, A. Royer, J. F. Kielkopf, and N. Feautrier, Phys. Rev. A **60**, 1021 (1999).
[33] L. Barbier and M. Cheret, J. Phys. B **16**, 3213 (1983).
[34] A. Kavokin, G. Malpuech, and F. P. Laussy, Phys. Lett. A **306**, 187 (2003).
[35] P. R. Eastham and P. B. Littlewood, Phys. Rev. B **64**, 235101 (2001).
[36] A. P. Alodjants *et al.*, Appl. Phys. B **89**, 81 (2007); J. Phys. B: At. Mol. Opt. Phys. **43**, 095502 (2010).